THE OFFICIAL MAGAZINE OF THE OCEANOGRAPHY SOCIETY

Oceanography

CITATION

Lucas, A.J., J.D. Nash, R. Pinkel, J.A. MacKinnon, A. Tandon, A. Mahadevan, M.M. Omand, M. Freilich, D. Sengupta, M. Ravichandran, and A. Le Boyer. 2016. Adrift upon a salinity-stratified sea: A view of upper-ocean processes in the Bay of Bengal during the southwest monsoon. *Oceanography* 29(2):134–145, http://dx.doi.org/10.5670/oceanog.2016.46.

DOI

http://dx.doi.org/10.5670/oceanog.2016.46

Adrift Upon a Salinity-Stratified Sea

A View of Upper-Ocean Processes in the Bay of Bengal During the Southwest Monsoon

By Andrew J. Lucas, Jonathan D. Nash, Robert Pinkel, Jennifer A. MacKinnon, Amit Tandon, Amala Mahadevan, Melissa M. Omand, Mara Freilich, Debasis Sengupta, M. Ravichandran, and Arnaud Le Boyer

Preparing a wave-powered Wirewalker profiler for a 13.5-day deployment from R/V *Roger Revelle* during the 2015 ASIRI-OMM southwest monsoon experiment in the northern Bay of Bengal. *Photo credit: San Nguyen*

> Co-located time series of temperature, salinity, velocity, optical properties, and turbulent microstructure measurements collected on board a drifting wave-powered profiler elucidated the patterns of upper-ocean variability and vertical heat and salt fluxes in the Bay of Bengal.

ABSTRACT. The structure and variability of upper-ocean properties in the Bay of Bengal (BoB) modulate air-sea interactions, which profoundly influence the pattern and intensity of monsoonal precipitation across the Indian subcontinent. In turn, the bay receives a massive amount of freshwater through river input at its boundaries and from heavy local rainfall, leading to a salinity-stratified surface ocean and shallow mixed layers. Small-scale oceanographic processes that drive variability in near-surface BoB waters complicate the tight coupling between ocean and atmosphere implicit in this seasonal feedback. Unraveling these ocean dynamics and their impact on air-sea interactions is critical to improving the forecasting of intraseasonal variability in the southwest monsoon. To that end, we deployed a wave-powered, rapidly profiling system capable of measuring the structure and variability of the upper 100 m of the BoB. The evolution of upper-ocean structure along the trajectory of the instrument's roughly two-week drift, along with direct estimates of vertical fluxes of salt and heat, permit assessment of the contributions of various phenomena to temporal and spatial variability in the surface mixed layer depth. Further, these observations suggest that the particular "barrier-layer" stratification found in the BoB may decrease the influence of the wind on mixing processes in the interior, thus isolating the upper ocean from the interior below, and tightening its coupling to the atmosphere above.

INTRODUCTION

The motivation for the US Air-Sea Interactions Regional Initiative (ASIRI) and India's Ocean Mixing and Monsoon (OMM) program lies in the lack of skill of numerical models to reproduce sea surface temperatures (SST) in the Bay of Bengal (BoB; Goswami et al., 2016, in this issue). Realistic SST is important for accurate representation of air-sea coupling and for forecasting intraseasonal monsoon fluctuations (Sengupta and Ravichandran, 2001; Joseph et al., 2005; Shankar et al., 2007; Chowdary et al., 2016). Much of the difficulty arises from the complex near-surface stratification in the region: mixed layer depths vary in time, and, more problematically for forecast models, over a broad range of spatial scales, from basin scale to sub-kilometer (and subgrid-scale) distances (Chowdary et al., 2016). A significant fraction of the spatial and temporal variability of mixed layer properties appears to be due to the horizontal advection of lateral near-surface variability, and is thus not amenable to forecasting by one-dimensional models of ocean-atmosphere coupling (Akhil et al., 2014; Benshila et al., 2014; Pant et al., 2015).

While large-scale ocean processes (e.g., 100 km scales and larger) are useful for assessing the atmospheric response to upper-ocean heat content in a laterally averaged sense (Shankar et al., 2007), processes that shape the character of upper-ocean stratification can occur on much smaller scales and influence smaller-scale air-sea exchanges (Friehe et al., 1991). This is particularly true in the BoB, where the volume of freshwater input per year, if spread over the entire 2.2 million square-kilometer surface area of the basin, would raise its level by two meters (Bhat, 2001; Sengupta and Ravichandran, 2001; Vinayachandran et al., 2002; Gopalakrishna et al., 2002; Papa et al., 2010). This freshwater flux, roughly equally split between river input and rain, is deposited unevenly in space and time. Although some of the exchange between relatively fresh and salty waters occurs in the seasonally reversing boundary currents (Jensen et al., and Lee et al., 2016, both in this issue), an important fraction occurs in the interior, where energetic mesoscale circulation and prevailing winds combine to redistribute these lateral gradients, in some cases sharpening them into ever-finer lateral gradients (Mahadevan et al., 2016, in this issue). Vertical circulations associated with these sharp submesoscale fronts can ultimately lead to irreversible exchange between fresh and oceanic waters, destroying small-scale lateral variability, and setting the average-upper ocean properties of the basin.

The Barrier Layer and the Bay of Bengal

A particularly important component of the upper-ocean structure in the BoB is the multi-layer stratification found during much of the year. This stratification is composed of a shallow halocline (typically found at 10–30 m depth) and a permanent thermocline, typically beginning at around 50 m depth and centered at ~100 m depth. The range of depths between the halocline and the thermocline is referred to as the "barrier layer," invoking the relative isolation of the waters at the thermocline and below from those processes that drive variability in the upper portion of the water column.

As the existence of the barrier layer depends on salinity stratification, and vertical salinity stratification in the BoB depends on the redistribution of lateral gradients in sea-surface salinity, it follows that ventilation of the interior, its biogeochemical characteristics, and its residual circulation all depend on the physical mechanisms that control the lateral redistribution of salinity in the surface ocean. These processes are most active during the periods of largest precipitation and river runoff, that is, during the southwest monsoon.

Thus, development of working knowledge of the complex mosaic of ocean variability in time and space during the southwest monsoon, and in particular the processes that control stratification and

Box 1. Observations of the Variability of the Deep Chlorophyll Maximum in the Bay of Bengal

By Andrew J. Lucas, Mara Freilich, Melissa M. Omand, and Amala Mahadevan

Deep chlorophyll maxima (DCMs), typically centered within the pycnocline, are found throughout the world ocean. First recognized as coherent features following the development of optical techniques for measuring chlorophyll fluorescence in situ, the advent of autonomous vehicles such as gliders and floats demonstrated their persistence and ubiquity. Our present understanding of DCMs implicates the organisms that form them as important players in ocean biogeochemical transformations and carbon cycling (e.g., Cullen, 2015). Although recognized as widespread and important, little is known regarding their in situ variability on small spatiotemporal scales. Observations gathered by sensors on the Wirewalker (WW) during the 2015 ASIRI program elucidate the exquisite small-scale vertical structure of chlorophyll found at depth (Figure 2c) and allow for comments regarding time variability within the BoB DCM.

Figure B1A shows the surface shortwave radiation recorded at a nearby mooring (Weller et al., 2016, in this issue), and Figure B1B shows the on-isopycnal chlorophyll concentration at the DCM (specifically across the 21.0 σ_t to 22.8 σ_t density range) over the first 3.5 days of the WW drift. The main DCM was centered at approximately 50 m depth, which coincided with the top of the permanent thermocline, just below the barrier layer, and the oxycline (Figure 2c, oxygen not shown). The depth of the primary DCM varied in time, primarily due to twice-daily oscillations of ~15 m in the depth of the pycnocline associated with the internal tide (Figure 2c). The intensity of the DCM varied on a diel (24 h) cycle, with maximum values found in the late afternoon (Figure B1B and Figure 2c).

Critically, our co-located measurements of temperature and salinity allowed mapping of chlorophyll to density surfaces rather than depth, which allowed separation of time variability in the DCM from variability associated with the heaving of internal waves.

Figure B1C shows a canonical 24 h time series of normalized surface shortwave radiation (the canonical maximum shortwave radiation over the period was 800 W m^{-2}), DCM time variability (calculated as the median chlorophyll fluorescence value across the 21.0–22.8 σ_t density range), a harmonic fit to that time series (using only daily and twice-daily coefficients), and the derivative of the harmonic fit (a measure of the instantaneous rate of change of chlorophyll fluorescence in the DCM). Nearly all of the variability in the canonical 24 h time series was well represented by this simple harmonic fit. The maximum of the rate of change in chlorophyll *a* fluorescence was coincident with the maximum in solar radiation, and resulted in accumulation of chlorophyll *a* in the early afternoon (roughly three hours after the peak shortwave radiation). The range of fluorescence variability was approximately 25% of the mean (Chl_{mean} = 1.3 µg L^{-1}, $\Delta_{canon}Chl$ = 0.31 µg L^{-1}).

We can make use of the canonical chlorophyll fluorescence time series as a crude metric of primary productivity (i.e., the rate of carbon fixation in the DCM). In doing so, we assume: (1) a linear relationship between chlorophyll fluorescence and chlorophyll concentration, and (2) a constant cellular carbon to chlorophyll concentration ratio (C:Chl). The first assumption is broadly true as long as non-photochemical quenching is minor (likely given the depth of the DCM and the observed pattern of maximum fluorescence during daylight hours). While the assessment of variability in carbon to chlorophyll ratios in the DCM is beyond the scope of our autonomous observations, water samples collected nearby during ship operations will ultimately provide information regarding this assumption. Other observations in tropical and subtropical oceans have shown generally weak diel C:Chl variability at the depth of the DCM (e.g., Marra, 1992; Le Bouteiller et al., 2003; Wang et al., 2009).

For the present, asserting that C:Chl is constant and has a value of 50:1 (e.g., Cullen, 1982; Cloern et al., 1995; Le Bouteiller et al., 2003), we arrive at a value of maximum daily productivity of 1.2 g C m^{-2} d^{-1}, where the volume-specific maximum daily rate has been integrated over the 20 m vertical extent of the DCM. The daylight-averaged productivity, integrated over the same layer, is 0.3 g C m^{-2} d^{-1}, similar to estimates of DCM productivity in other tropical DCMs. The daylight-averaged productivity is perhaps more robust than any instantaneous estimate, since it only assumes a constant daily averaged C:Chl ratio, rather than the simultaneous production of carbon and chlorophyll on short time scales.

The time and depth distribution of mixing derived from data from the temperature microstructure sensor aboard the WW, when combined with an average shipboard-derived nitrate-depth relationship (not shown), permits a rough comparison between the above-calculated

mixing, is a prerequisite for understanding both regional ocean/atmosphere coupling and the general circulation and biogeochemisty of the BoB.

Our progress toward understanding these processes is probably most impeded by our lack of observations on the appropriate spatiotemporal scales. Although there is a robust history of oceanographic exploration in the BoB region, and increasing efforts by local nations to conduct both regular shipboard surveys and prolonged time-series observations at open-ocean moorings, observation of small-scale, rapidly evolving physical processes remains a difficult measurement problem, requiring intense observational effort (see MacKinnon et al., Shroyer et al., and Sarkar et al., 2016, all in this issue).

This article provides an overview of upper-ocean variability in the BoB from the point of view of a rapidly profiling vehicle deployed from R/V *Roger Revelle* that drifted in a cyclonic mesoscale eddy during the 2015 southwest monsoon (August 29 to September 11, 2015). Equipped with a variety of sensors, the profiler followed the mesoscale flow while making rapid cycles to 105 m depth. In all, 2,414 profiles with an average repeat rate of ~7.5 min were collected, resulting in a unique 13-day record of the evolution of the upper ocean from a mesoscale stream-wise perspective. The record elucidates the characteristics of the mixed

productivity rate and that of "new" productivity due to nitrate flux into the DCM, where the quantity of interest is the vertical divergence of nitrate flux. There is some possibility that the DCM in the BoB is at times nitrate-limited, as the depths that coincide with the DCM have a range of values between 0 to ~3 µmol NO_3 L^{-1}. We can estimate flux divergence of nitrate at the DCM using a diffusivity of 10^{-6} m^2 s^{-1} derived from the WW data (Figure 5) and a vertical nitrate gradient of ~3×10^{-4} g N m^{-5} based on a bay-wide, 64-cast survey of nitrate concentrations with depth yields 2 mg N m^{-2} d^{-1} of nitrate input into a 20 m thick DCM per day. This number is roughly an order of magnitude smaller than the daylight-averaged demand of 50 g N m^{-2} d^{-1} calculated from the diel change in chlorophyll fluorescence with a Redfield ratio C:N conversion of 6.6:1. It is, however, perhaps a reasonable lower bound of the background new production at the DCM during quiescent periods (a Redfield-scaled new production rate of ~15 mg C m^{-2} d^{-1}). Episodic events such as cyclones, advection by eddies and submesoscale instabilities (e.g., Figure 5, Period II), and along-isopycnal mixing may account for much of the total bay-wide new production (just as they presumably account for much of the water mass modification in the basin). Nevertheless, the strong stratification and weak mixing captured here is suggestive of an efficiently recycled community in the DCM (see also Sarma et al., 2016, in this issue).

Taken together, these observations suggest that the DCM, while perhaps a relatively weak sink for carbon in an average, one-dimensional sense, is a vibrant, tightly linked community of autotrophs and heterotrophs capable of rapid biochemical transformations. As the number and quality of concurrent measurements of physical and biogeochemical proprieties and rates increase, much more about these important communities, and their contribution to the global carbon cycle, is likely to be learned.

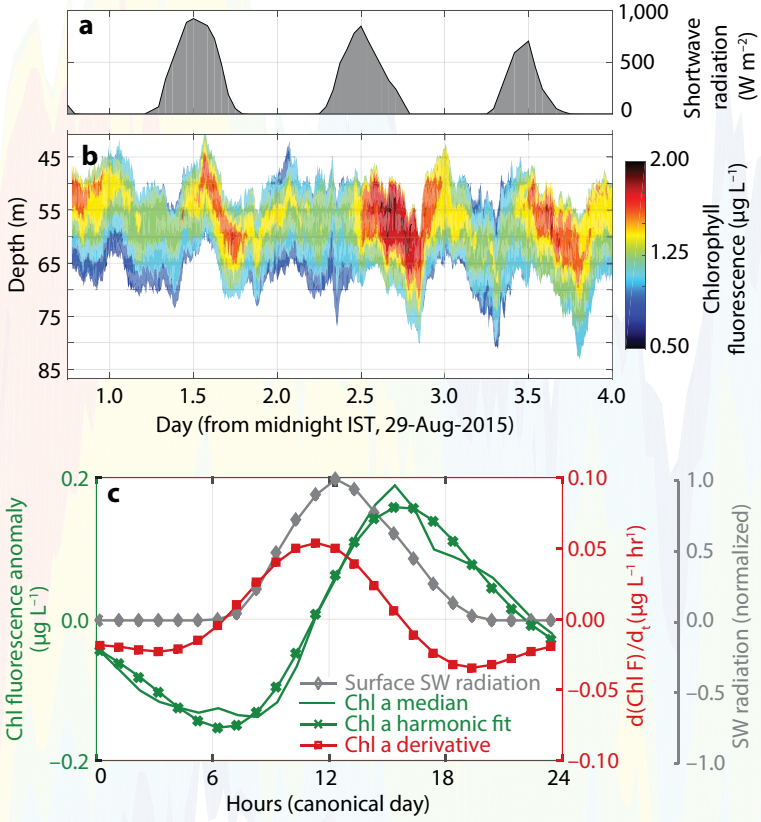

FIGURE B1. Diel variability in the Bay of Bengal deep chlorophyll maximum (DCM). (A) Surface irradiance, measured at a nearby air-sea flux mooring, shows the daily variability of shortwave radiation during the first ~3 days of Wirewalker drift. (B) On-isopycnal chlorophyll fluorescence, projected onto depth, demonstrates the large vertical excursions of the DCM with the internal tide as well as daily variability in its chlorophyll concentration. Observing DCM chlorophyll intensity in a density-following frame of reference eliminates variability due to vertical internal wave heaving. (C) A canonical 24 h time series of chlorophyll variability was calculated from the median chlorophyll value across the 21.0 σ_t and 22.8 σ_t density range, producing a "typical" 24 h cycle. A harmonic fit to that canonical time series shows the dominance of the diel cycle in chlorophyll, with a maximum rate of change coincident with maximum surface irradiance. The rapid temporal cycling implies tight coupling between DCM autotrophs and heterotrophs, and the dominance of recycled nutrients over primary production there.

layer, the near-surface halocline, the barrier layer, and the upper portion of the continuously stratified thermocline. Furthermore, the observations permit quantitative assessment of salt and heat fluxes in a temporally continuous framework, and show the importance of both local and nonlocal sources of variability in those fluxes. Ultimately, we expect that these types of observations will improve air-sea coupling in prognostic models of the monsoon in South Asia.

THE ASIRI WIREWALKER

The Wirewalker (WW; see photo on title page) is a profiling vehicle developed at the Scripps Institution of Oceanography (Rainville and Pinkel, 2001; Pinkel et al., 2011; Smith et al., 2012; http://www.delmarocean.com). Its motive force is provided by the surface wind-wave field, which drives the vehicle and sensor package down a wire suspended from a surface buoy. At the limit of the profiling range, the vehicle is mechanically decoupled from the wire, and it rises smoothly toward the surface under its own buoyancy. Because no onboard energy is required for profiling, extended deployments are possible. A ~50 kg (in air) instrument and battery payload enable continuous sampling of a range of ocean properties, including temperature and salinity, bio-optical variability and dissolved oxygen saturation, turbulent dissipation rate, and velocity profiles. For example, on the 13-day deployment described here, temperature, salinity, pressure (RBR CTD), dissolved oxygen (Alec Electronics RINKOIII oxygen optode), and three bio-optical channels (Turner Designs Cyclops 7 chlorophyll *a* fluorescence, chromophoric dissolved organic material [CDOM] fluorescence, and turbidity) were sampled continuously at 6 Hz. Horizontal currents were sampled continuously at 16 Hz (Nortek Aquadopp II), and microstructure temperature and vehicle acceleration were recorded continuously at 100 Hz (Oregon State University χpod; Moum and Nash, 2009). The total drift data set consists of greater than 600 million individual observations. For analysis, quantities in individual profiles were decimated to 25 cm vertical resolution from 2 m to 105 m depths.

We deployed the WW in the central region of a poorly structured cyclonic mesoscale eddy (Figure 1), in association with an autonomous SOLO-II float (χSOLO; see Shroyer et al., 2016, in this issue). Over two weeks, the eddy became increasingly organized, and correspondingly, the mesoscale velocities accelerated. The predominant near-surface property variability in the area was a northeast-to-southwest-trending, 100 km wide region of low salinity (as shown by shipboard surveys, Figure 1) that was entrained between the cyclonic eddy to the south and a strong anticyclonic eddy to the northwest, but not fully aligned with the evolving mesoscale streamlines. This mismatch of mesoscale streamlines and near-surface lateral salinity variability resulted in a WW trajectory that followed the average mesoscale velocity over the upper 100 m, cutting through a number of regions of small-scale lateral variability in the surface ocean (Figure 1). The relative motion allowed an assessment of the degree of decoupling between the upper ocean and waters below for a number of different upper-ocean stratification regimes, atmospheric forcing types, and degrees of near-surface lateral stratification, while concurrently tracking

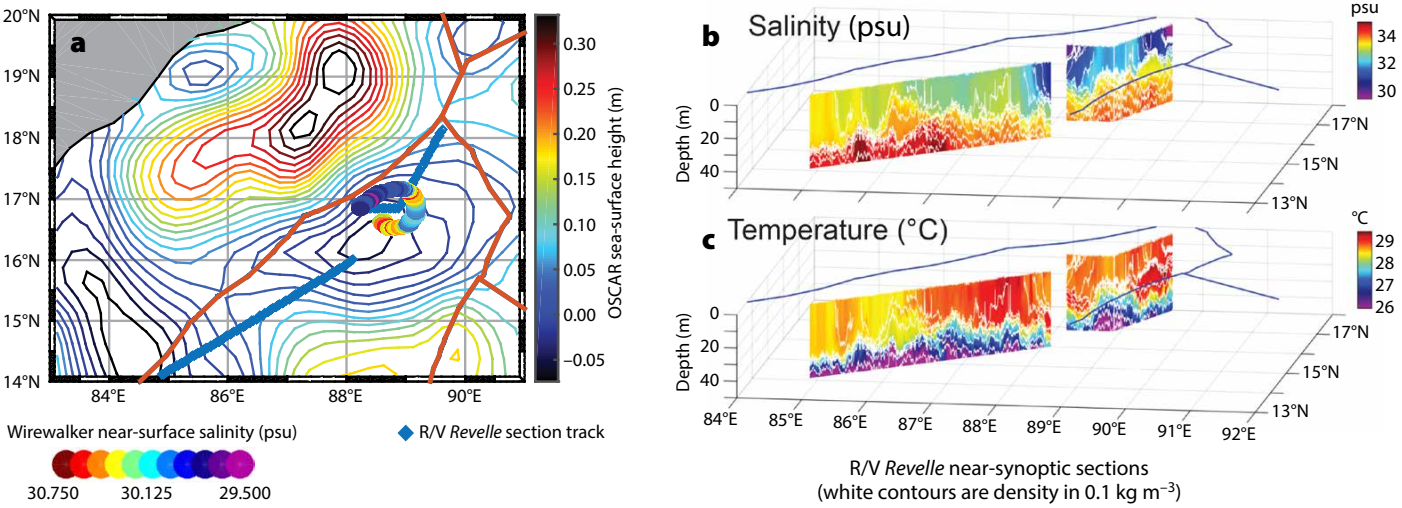

FIGURE 1. Mesoscale conditions in the northern Bay of Bengal during the 13-day Wirewalker (WW) drift. (a) The sea surface height (SSH) field shows the large cyclonic feature occupying the northern portion of international waters on September 8, 2015, after the feature had become well organized (see text). The WW followed the evolving mesoscale conditions over its 260 km drift, crossing several near-surface fronts (as seen by the near-surface salinity gradients along the WW track). At the conclusion of the 2015 southwest monsoon field operations, we occupied a 650 km section across the cyclonic eddy (blue line) with a rapid profiling shipboard survey system (the Scripps Institution of Oceanography Fast CTD). (b) Salinity in the upper 50 m shows the northeast/southwest-trending low-salinity feature north of the eddy center, and west-to-east transport of low-salinity waters south of the eddy center. These patterns in upper-ocean salinity were echoed by variability in upper-ocean temperature (c), illustrating the strong lateral variability in heat content during the southwest monsoon. The red lines (left panel) and blue lines (right panel) indicate the boundaries of the regional Exclusive Economic Zones (EEZs).

the time evolution of the stratified interior stream-wise along the eddy trajectory. This combined, concurrent, and continuous record of temperature, salinity, velocity, shear, and turbulent microstructure is among the first of its kind in the region (see Shroyer et al., 2016, in this issue, for another example).

STRATIFICATION, SHEAR, AND UPPER-OCEAN DECOUPLING

Stratification

The near-surface stratification during the drift was dominated by salinity gradients, with mixed layer salinity values below 30 psu throughout (Figure 2a). The main thermocline began at approximately 50 m depth and continued through 150 m depth (Figures 1 and 2b). The two regions of strong stratification were separated by a 20 m thick, relatively homogenous barrier layer of approximately 32 psu and 29°C (Figure 2a,b). For most of the record, the barrier layer registered the maximum temperature in each profile, reflecting the presence of a vertical temperature inversion. This was particularly apparent in the latter portion of the record, where the surface temperature was nearly 1.5°C cooler than that at 30 m depth (Figure 2b). The rapid changes in near-surface stratification, for example, at day 8.5 (Figure 2b), were associated with the WW drift crossing shallow surface fronts with scales of <10 km. These fronts, although relatively strong in terms of lateral density gradient (up to 0.5 kg m^{-3} over 10 km), were also partially temperature-compensated, implying a good deal of lateral SST gradient. These lateral gradients in SST were on the order of 1°C to 1.5°C (Figures 1b,c and 2b), perhaps not coincidentally similar to the vertical gradient between SST and the barrier layer below. Although the role lateral SST variability plays in small-scale air-sea interactions in the BoB is at present poorly characterized, one consequence is that it renders one-dimensional models ineffective at predicting Eulerian measurements of SST gathered at long-term moorings (Sengupta and Ravichandran, 2001).

Mixed layer depth changed significantly over the course of the drift, from ~30 m depth in the center of the eddy to <10 m depth during the frontal crossing on day 8.5 (Figure 2a,b). The barrier

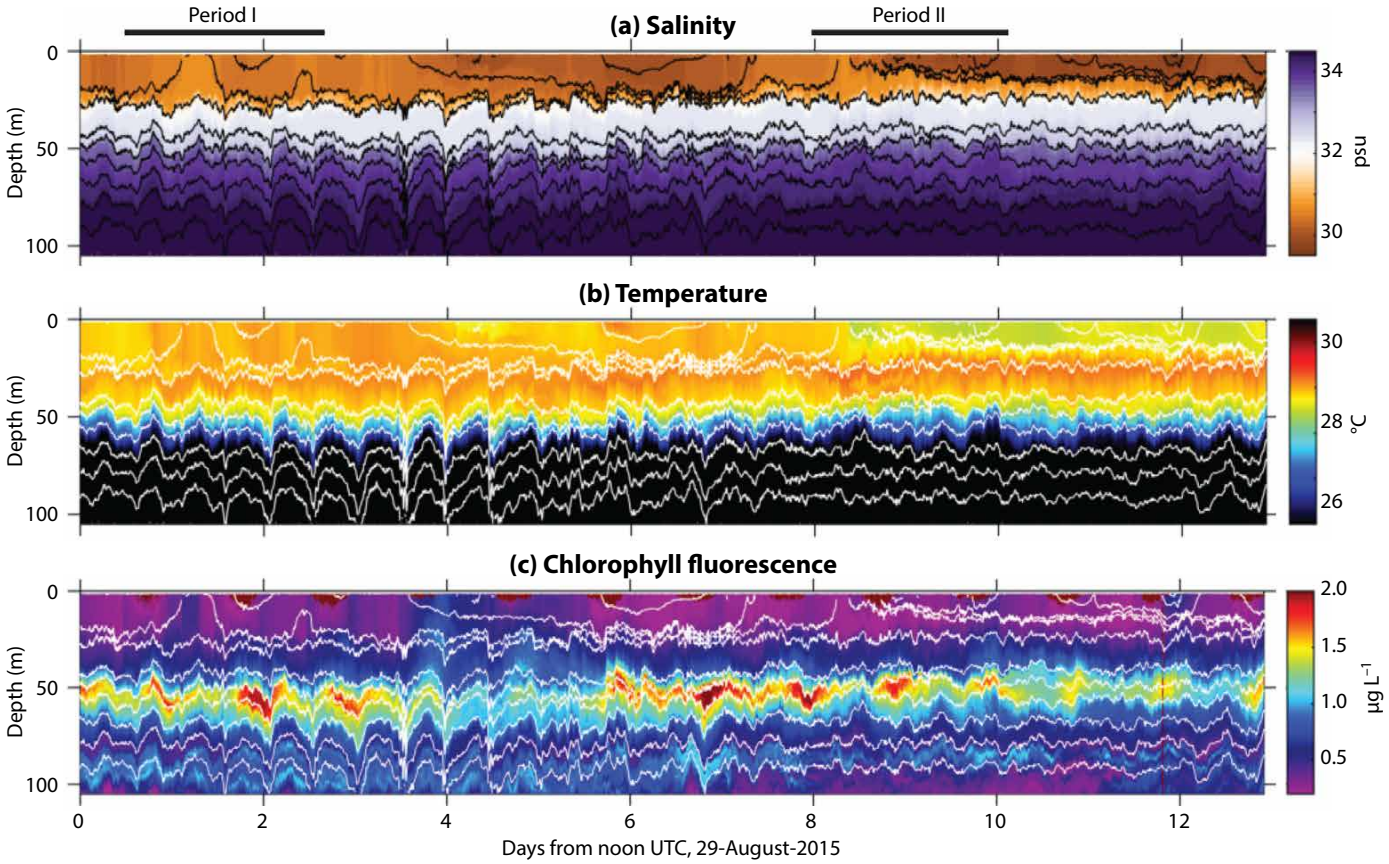

FIGURE 2. Along-track time series of (a) temperature, (b) salinity, and (c) chlorophyll fluorescence from the Wirewalker profiler. Black (white) isolines of constant density separated by 0.2 kg m^{-3} are shown in each panel. A barrier layer of a relatively constant T-S (temperature-salinity) composition was present throughout the drift, centered at 40 m depth. The upper-ocean stratification was dominated by salinity; the misalignment of the lateral salinity gradients near the surface and the mesoscale flow allowed the WW to cross a number of near-surface fronts, in particular, centered on day 8.5 (discussed in the text). Chlorophyll fluorescence, in particular the fine-scale structures apparent between 90 m and 100 m depth, which were coherent over days and over >100 km distance, demonstrate the weak mixing in the thermocline over the course of the drift. Period I and Period II, noted with overbars, are discussed in the text.

layer, however, changed relatively little in terms of depth, extent, or characteristic temperature and salinity, with the notable exception of below the front on day 8.5 (see the following section). The thermocline and waters below also demonstrated very little variability outside of vertical displacements associated with the internal tide. Taken as a whole, a qualitative picture emerged of a highly variable but shallow surface boundary layer (< ~30 m) overlying a barrier layer and a quiescent interior.

Shear

The WW ascends to the surface decoupled from the wavefield that propelled it downward, and thus is a stable platform for collection of vertically well-resolved currents, velocity shear, and turbulent microstructure. GPS and Iridium telemetry tracked the WW so that the currents as measured relative to the profiler could be transformed to a frame of reference relative to Earth. The observations collected during this drift showed some salient features of the flow field, in particular with regard to the relative lack of coupling between near-surface and deeper waters.

The mesoscale velocity field and semidiurnal internal tide (Figure 3a) dominated the depth-mean velocity (over the 105 m profile length). Neither class of motion contributed in an obvious way to vertical shear in velocity, which was instead dominated by the near-inertial band early in the record, and, seemingly, by the strong lateral gradients observed in the second half of the record.

Near-inertial variability is one of the primary pathways of oceanic mixing, owing to its characteristically strong shear (e.g., Alford, 2003). During this drift, near inertial oscillations reaching velocities >40 cm s^{-1} were present in the mixed and barrier layers (Figure 3b,c). Below, bands of near-inertial variability with upward phase propagation (and therefore downward energy propagation) were apparent in the thermocline, particularly at the beginning of the drift (days 0 to 4; Figure 3b,c).

Near-inertial variability is typically modeled schematically as an oscillating mixed layer slab near the surface and vertically radiating near-inertial

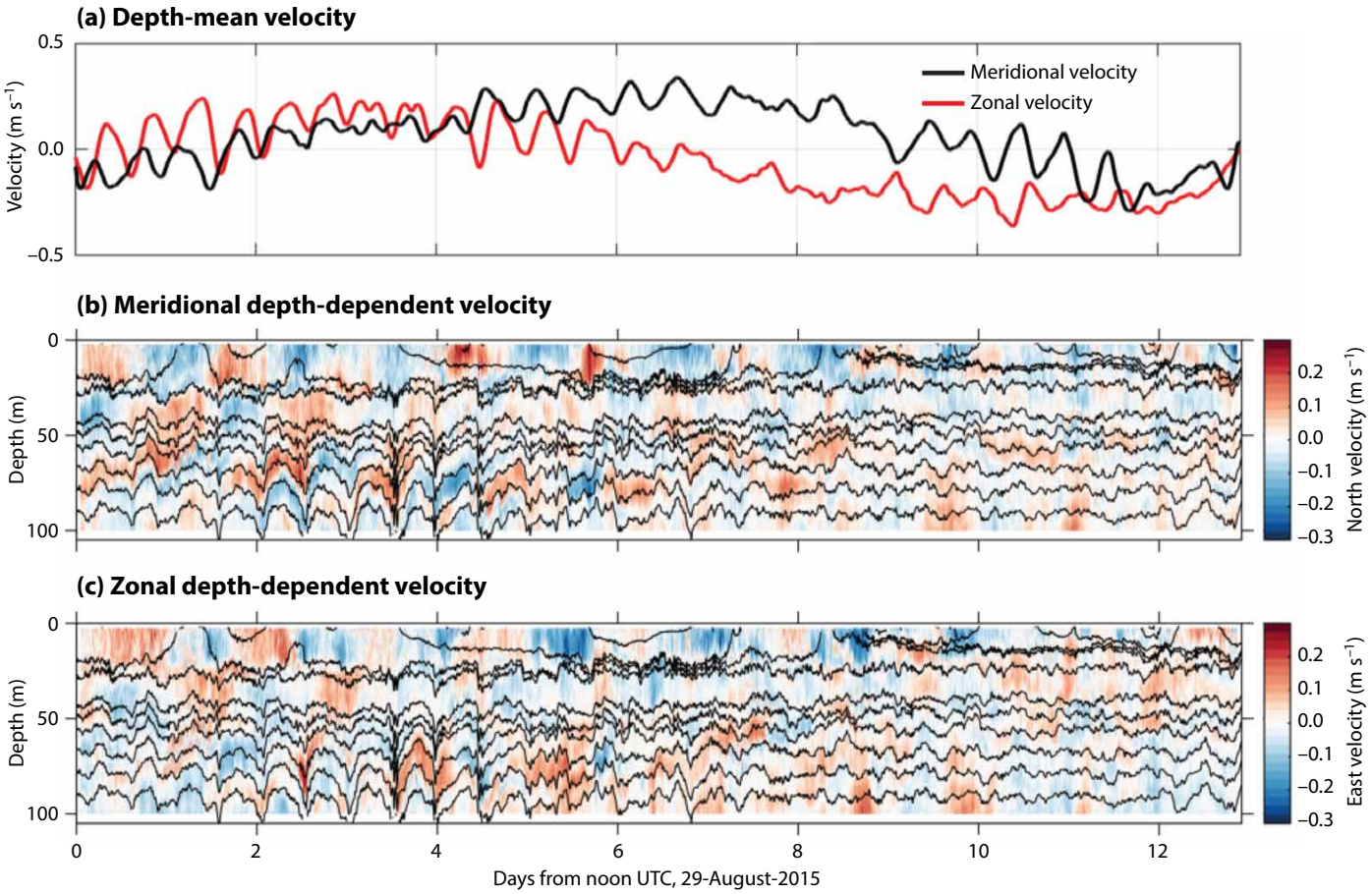

FIGURE 3. Along-track time series of (a) depth-mean meridional and zonal velocities, (b) depth-dependent meridional velocities, and (c) depth-dependent zonal velocities from a single point current meter affixed to the Wirewalker profiler. Depth-mean velocities were dominated by the mesoscale and semidiurnal fluctuations associated with a propagating low-mode internal tide. Depth-dependent velocities, and thus shear, showed the imprint of energetic near-inertial oscillations with upward phase propagation in the thermocline. Near-inertial shear was enhanced at the base of the mixed layer but not at the interface between the barrier layer and the stratified interior. This decoupling between the upper ocean and the thermocline may be due to the characteristic two (or more) layer stratification of the Bay of Bengal.

waves below. Shear is elevated at the base of the mixed layer and at intervals of the near-inertial vertical wavelength at depth. Energy that is not lost to shear-driven mixing locally can propagate into the abyssal ocean.

The observations of shear gathered during the WW drift suggest a potentially intriguing modification to this schematic understanding for systems such as the BoB, which are characterized by multi-layer stratification. The near-inertial oscillations in the mixed and barrier layers were 180° out of phase (thus creating strong shear at the mixed layer base), but the same was not true between the barrier layer and the continuously stratified thermocline (Figures 3b,c and 4a; note, for example, the difference in meridional velocity between 20 m and 40 m depth and 40 m and 60 m depth). The suggestion is that the barrier layer was also responding as a slab to near-inertial motions, but, while shear was elevated at the base of the mixed layer, it was not elevated at the base of the barrier layer. If broadly true, this asymmetry in shear might help explain the tendency for the BoB to have weak turbulent mixing (see also Shroyer et al., MacKinnon et al., and Jinadasa et al., 2016, all in this issue), and to form a consistent barrier layer-type upper-ocean stratification in the face of major lateral gradients, while simultaneously isolating the thermocline from property exchange with the ventilated surface layers (see Johnston et al., 2016, in this issue for further discussion of near-inertial-variability in the BoB).

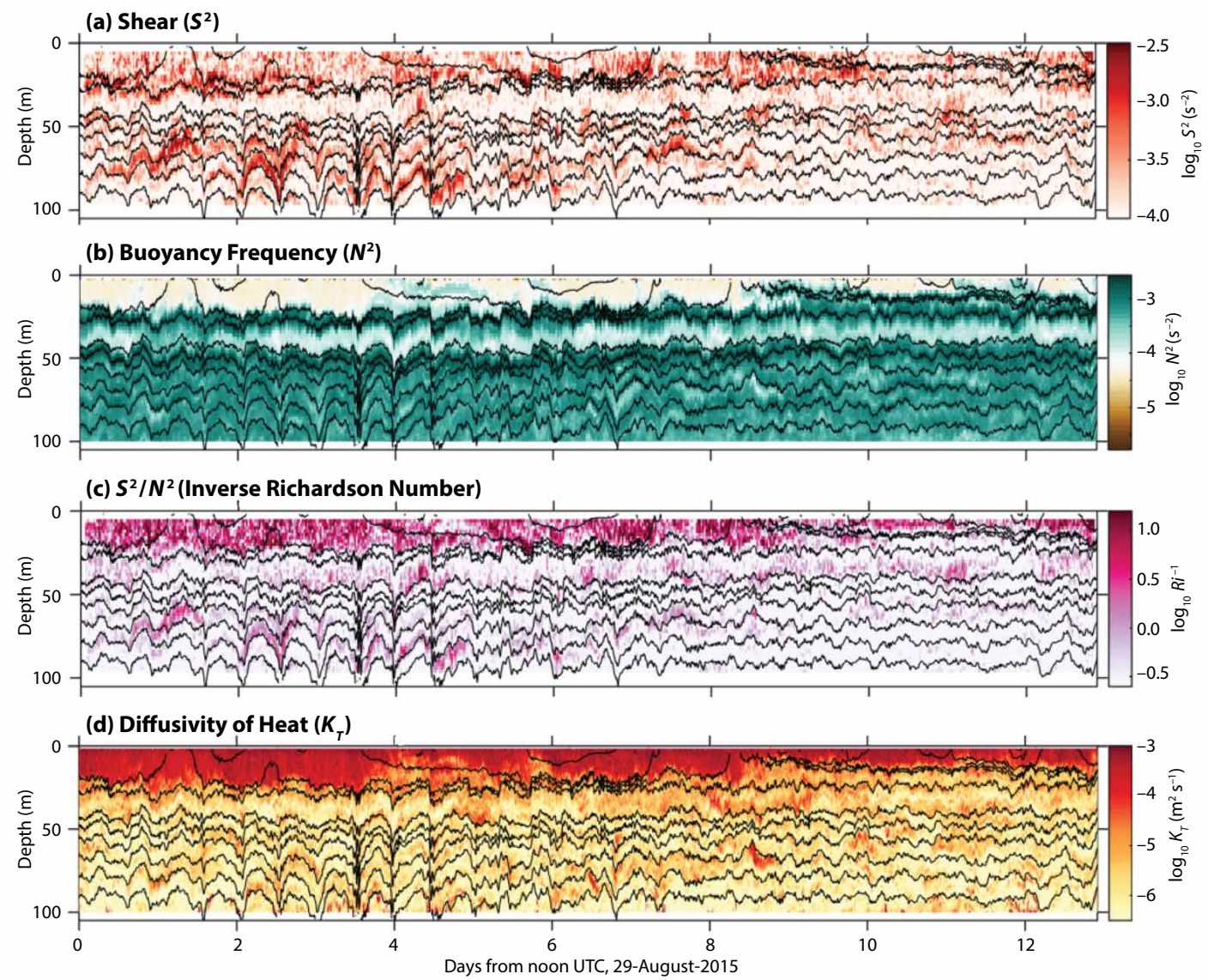

FIGURE 4. (a) Vertical squared-shear, (b) buoyancy frequency, and (c) inverse Richardson number (*Ri*) calculated from Wirewalker profiler data. This parameterization of the water column's susceptibility to shear-driven mixing is broadly consistent with the patterns of the magnitude of the diffusivity of heat as estimated from microstructure temperature recorded onboard the Wirewalker. In particular, the importance of near-surface stratification to the depth of the actively mixing mixed layer is apparent in both *Ri* and dissipation rate of turbulent kinetic energy (not shown) and diffusivity of heat (K_T). The correspondence between K_T and *Ri* in the thermocline during near-inertial shear events highlights the consistency of these independent observations.

Mixing, Barrier Layers, and Upper-Ocean Decoupling

The susceptibility of a stratified water column to destabilization by vertical shear can be parameterized by the gradient Richardson number (*Ri*). This unitless number is a ratio of the local buoyancy frequency (N^2) to the squared vertical shear (S^2). Over the course of the WW drift, S^2 was at a maximum at the base of the mixed layer and in upward-propagating bands in the thermocline, both of which were driven by near-inertial variability. Stratification, and therefore N^2, displayed two- and three-layer vertical structure (days 0–8.5 and days 8.5–13, respectively).

The WW was equipped with a χpod microstructure temperature sensor, which captures temperature variance in the inertial and viscous convective subranges (Moum and Nash, 2009). These measurements can in turn be used to estimate the dissipation rate of turbulent kinetic energy (not shown) and diffusivity of heat (K_T). A comparison of the distribution of *Ri* and K_T along the WW drift shows a broad correspondence. While both quantities are inversely proportional to stratification, microstructure measurements are independent from measurements of vertical shear on "large" (i.e., meter and larger) scales. Thus, the suggestion that shear associated with near-inertial waves may drive elevated mixing in the thermocline, inferred from the presence of supercritical *Ri* numbers (shown as regions of warm colors in Figure 4c), was borne out independently by estimates of mixing from microstructure temperature (Figure 4d).

Weak stratification led to elevated mixing rates in the mixed layer, even in the presence of little near-inertial shear. Both *Ri* number analysis and diffusivity estimates showed the importance of changes in mixed layer depth associated with lateral gradients in salinity stratification to the vertical extent of near-surface mixing. Both also supported the hypothesis that shear-driven mixing found at the base of the mixed layer was absent from the interface of the barrier layer and the thermocline below, indicating decoupling of the near-surface in the BoB from the interior.

VERTICAL FLUXES WITHIN THE BARRIER LAYER: A ROLE FOR SUBMESOSCALE FRONTS?

The 2,414 profiles of temperature microstructure and temperature and salinity fine structure gathered over a 13-day period allowed for quantitative characterization of the vertical fluxes of heat and salt. These fluxes were on average very small in the mixed layer as well as in the barrier layer and the thermocline below. For example, deployment-averaged heat fluxes were only ~2 W m^{-2} in the mixed layer, <1 W m^{-2} in the barrier layer, and gradually increased to −5 W m^{-2} at 100 m depths (data not shown). Thermocline diffusivities averaged 10^{-6} m^2 s^{-1} below the barrier layer and not much higher at and above it (below the surface mixed layer). That is, during this particular average of southwest monsoon conditions, mixing rates were below typical ocean values (~10^{-5} m^2 s^{-1}), and the fluxes were correspondingly small. There appeared to be one slight modification to that background state, which is illustrated in Figure 5. The interior heat fluxes reported here are small compared to atmospheric fluxes, suggesting that (1) the mixed layer responds directly to atmospheric forcing on a daily cycle with little internal redistribution of heat by turbulence (see Shroyer et al., 2016, in this issue, for a discussion of diurnal heating dynamics), (2) lateral advective processes are important in redistributing heat, or (3) interior mixing occurs in isolated, intense events, such as beneath the front that was sampled here, which is spatially localized but persistent in time, or other nonlinear features such as the bore reported in Sarkar et al. (2016, in this issue).

> "We expect that the quantitative assessment of these mechanisms will ultimately provide better prediction of sea surface temperature and the associated air-sea coupling over the Bay of Bengal, yielding increased fidelity in monsoon weather forecasting for South Asia."

The Barrier Layer and the Dynamics Above

It is instructive to compare segments of the WW record over the course of the drift from the perspective of heat and salt fluxes. The first period (days 0.5–2.5, indicated as an overbar in Figure 2a) was collected within the forming core of a cyclonic eddy, and was characterized by a deployment-maximum mixed layer depth of 30 m. In contrast, the second period (days 8–10; also indicated with an overbar in Figure 2a) coincided with a crossing of a strong lateral gradient in salinity and a deployment-minimum in mixed layer depth. The two periods bridged an active phase of the southwest monsoon (south-southwest winds at 5–8 m s^{-1}; wind stress of 0.1–0.3 N m^{-2}) and a break phase (westerly winds under 5 m s^{-1}; wind stress <0.1 N m^{-2}; Figure 5a).

Forty-eight-hour average mixed layer heat fluxes in Period I were small (−1.5 W m^{-2}, where the sign convention is negative for downward heat flux; Figure 5d), with a clear signal of diurnal heating and cooling that was essentially balanced over a daily cycle (see

Shroyer et al., 2016, in this issue). The surface boundary layer had diffusivities of ~10^{-4} m^2 s^{-1} and greater (Figure 5d), rapidly tapering off across the base of the surface layer and into the barrier layer. Thermocline diffusivities were generally <10^{-6} m^2 s^{-1}. Instantaneous downward heat flux associated with bands of near-inertial shear was of similar magnitude to the downward heat flux during the heating portion of the diurnal cycle, although the integrated near-inertial heat flux was far less than the integrated atmospheric fluxes. Salt flux was weak and peaked at the base of the mixed layer.

In contrast, the patterns of 48-hour-averaged heat and salt fluxes during Period II were quite different. Shallow salinity stratification after the front crossing on day 8.5 led to a shallow mixed layer, with diffusivities dropping off rapidly below 10 m (contrast diffusivities in Periods I and II in Figure 5d, left-hand panel). Temperature and

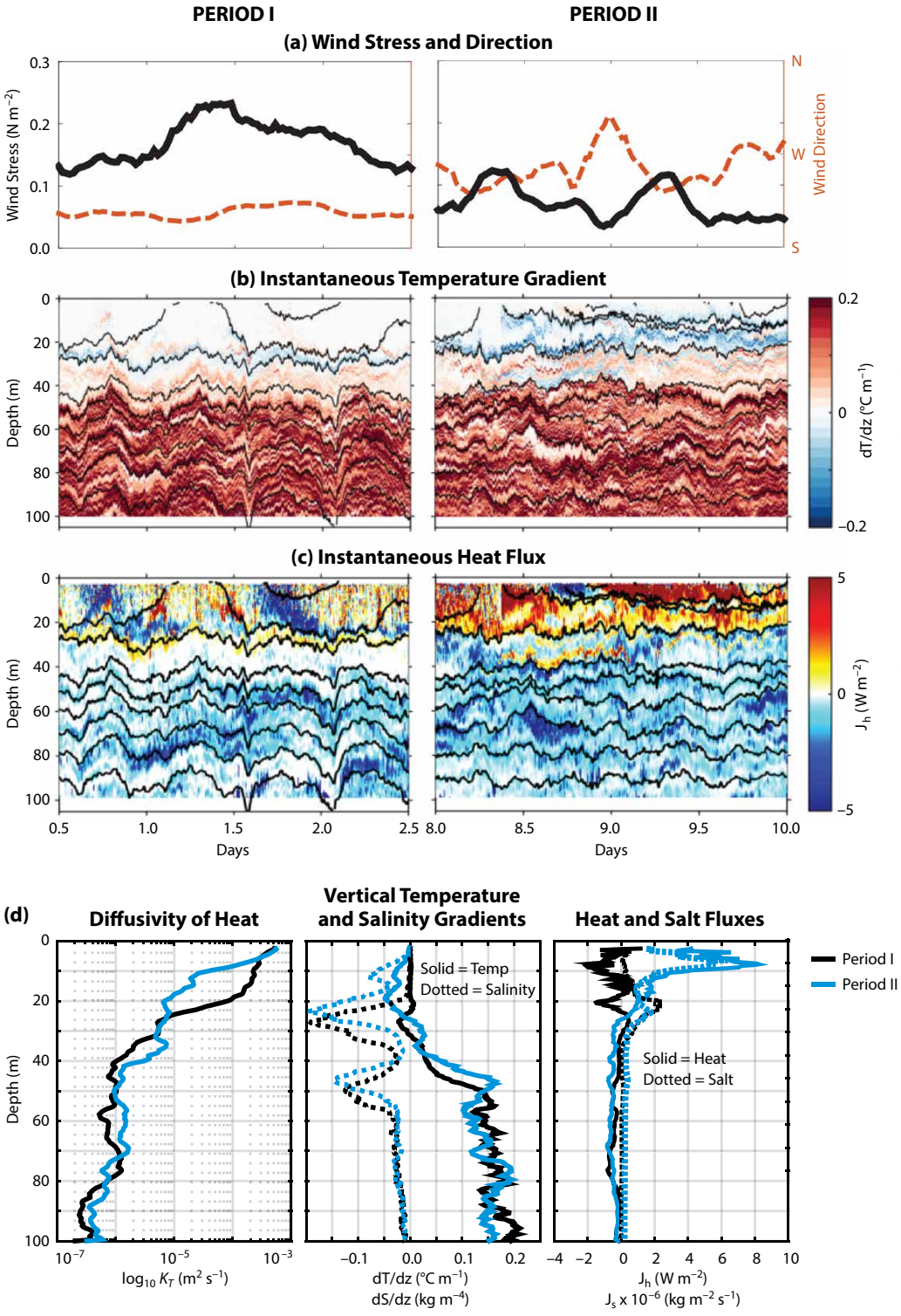

FIGURE 5. A comparison of fluxes between a region with a relatively deep mixed layer in the central part of a poorly organized cyclonic eddy and a region of strong lateral gradients and shallow mixed layers along the eddy edge. The two regions were sampled during the active phase (Period I) and inactive phase (Period II) of the southwest monsoon, as reflected by the wind stress and direction (a). Away from the mixed layer, diffusivities were weak, falling below 10^{-6} m^2 s^{-1} deeper than 40 m (in 48 h averages, left panel in (d)). While the barrier layer was quiescent during Period I (and most of the drift), elevated diffusivities in the barrier layer were observed coincident with the region of maximum lateral stratification (Period II). An interesting hypothesis is that ageostrophic processes associated with the front drove fluxes in the barrier layer, even as those same processes, by converting lateral variability into vertical stratification, are ultimately responsible for the barrier layer, and thus the degree of decoupling between the near-surface and the thermocline and below.

salinity gradients were large at the base of the mixed layer, and the corresponding estimated fluxes of those quantities were elevated, reaching >6–8 W m^{-2} and >5 × 10^{-6} kg m^{-2} s^{-1} for heat and salt fluxes across the mixed layer base, respectively. The near-surface heat flux (5 W m^{-2}) was of the opposite sign to that measured in Period I. The strong, ageostrophic shear associated with the frontal dynamics around day 8.5 apparently contributed to this elevated mixing (see the instantaneous heat flux estimates around this time; Figure 5c).

Below the mixed layer, the story in Period II continued to deepen. Diffusivities in the barrier layer (centered on 40 m depth) are an order of magnitude higher than those during Period I (and remain elevated into the thermocline; Figure 5d). This was the case despite the weaker wind forcing (Figure 5a), relative paucity of near-inertial shear (Figure 3), weak internal tides (Figure 3), and relatively stronger stratification above (Figure 2). Although speculative, there appears to be a link between the processes associated with the narrow front in the very near surface and the barrier layer below, a feature that is in general resistant to the typical sources of open-ocean mixing in low latitudes. Thus, potentially, much of the (weak) exchange that occurs between the upper layers of the BoB and the barrier layer/thermocline may occur at sharp lateral gradients, even as those lateral gradients, and the processes they drive, are ultimately responsible for the particularly strong, multilayer stratification of the BoB.

CONCLUSIONS

Co-located time series of temperature, salinity, velocity, optical properties, and turbulent microstructure measurements collected on board a drifting wave-powered profiler elucidated the patterns of upper-ocean variability and vertical heat and salt fluxes in the Bay of Bengal. Upper-ocean stratification was dominated by salinity, which is ultimately derived from freshwater input at the boundary of the basin and from the atmosphere. Turbulent exchanges between the upper ocean and the stratified interior were generally weak, with heat fluxes typically <1 W m^{-2} passing through the stratified barrier layer. Near-inertial shear was elevated at the base of the mixed layer but not between the barrier layer and the continuously stratified interior. This suggests that multi-layer stratification may dampen the capacity of near-inertial oscillations to drive vertical exchange in the upper ocean in salinity-structured systems such as the BoB. The only evidence of significant exchange across the barrier layer occurred below a strong front, during which time-averaged heat fluxes exceeded 5 W m^{-2}. Similarly, the sign of the surface mixed layer heat flux changed from negative (downward) to positive (upward) in the vicinity of the front. This suggests that dynamics specific to sharp, small-scale fronts may be important to the vertical redistribution of properties in the Bay of Bengal, even through and below the barrier layer. The same dynamics may also control the redistribution of horizontal salinity gradients and establishment of the salinity stratification that constrains ocean-atmosphere interactions to the very near surface. We expect that the quantitative assessment of these mechanisms will ultimately provide better prediction of sea surface temperature and the associated air-sea coupling over the Bay of Bengal, yielding increased fidelity in monsoon weather forecasting for South Asia.

REFERENCES

Alford, M. 2003. Improved global maps and 54-year history of wind-work on ocean inertial motions. *Geophysical Research Letters* 30(8):1,424–1,427, http://dx.doi.org/10.1029/2002GL016614.

Akhil, V.P., F. Durand, M. Lengaigne, J. Vialard, M.G. Keerthi, V.V. Gopalakrishna, C. Deitel, F. Papa, and C. de Boyer Montégut. 2014. A modeling study of the processes of surface salinity seasonal cycle in the Bay of Bengal. *Journal of Geophysical Research* 119:3,926–3,947, http://dx.doi.org/10.1002/2013JC009632.

Bhat, G.S., 2001. Near surface atmospheric characteristics over the North Bay of Bengal during the Indian summer monsoon. *Geophysical Research Letters* 28:987–990, http://dx.doi.org/10.1029/2000GL012455.

Benshila, R., F. Durand, S. Masson, R. Bourdallé-Badie, C. de Boyer Montégut, F. Papa, and G. Madec. 2014. The upper Bay of Bengal salinity structure in a high-resolution model. *Ocean Modelling* 74:36–52, http://dx.doi.org/10.1016/j.ocemod.2013.12.001.

Chowdary, J.S., A. Parekh, S. Ojha, C. Gnanaseelan, and R. Kakatkar. 2016. Impact of upper ocean processes and air–sea fluxes on seasonal SST biases over the tropical Indian Ocean in the NCEP Climate Forecasting System. *International Journal of Climatology* 36:188–207, http://dx.doi.org/10.1002/joc.4336.

Cloern, J.E., C. Grenz, and L. Vidergar-Lucas. 1995. An empirical model of the phytoplankton chlorophyll: Carbon ratio—the conversion factor between productivity and growth rate. *Limnology and Oceanography* 40(7):1,313–1,321, http://dx.doi.org/10.4319/lo.1995.40.7.1313.

Cullen, J. 1982. The deep chlorophyll maximum: Comparing vertical profiles of chlorophyll *a*. *Canadian Journal of Fisheries and Aquatic Sciences* 39(5):791–803, http://dx.doi.org/10.1139/f82-108.

Cullen, J. 2015. Subsurface chlorophyll maximum layers: Enduring enigma or mystery solved? *Annual Review of Marine Science* 7:207–239, http://dx.doi.org/10.1146/annurev-marine-010213-135111.

Friehe, C.A., W.J. Shaw, D.P. Rogers, K.L. Davidson, W.G. Large, A.A. Stage, G.H. Crescenti, S.J.S. Khalsa, G.K. Greenhut, and F. Li. 1991. Air-sea fluxes and surface layer turbulence around a sea surface temperature front. *Journal of Geophysical Research* 96(C5):8,593–8,609, http://dx.doi.org/10.1029/90JC02062.

Gopalakrishna, V.V., V. Murty, D. Sengupta, S. Shenoy, and N. Araligidad. 2002. Upper ocean stratification and circulation in the northern Bay of Bengal during southwest monsoon of 1991. *Continental Shelf Research* 22(5):791–802, http://dx.doi.org/10.1016/S0278-4343(01)00084-X.

Goswami, B.N., S.A. Rao, D. Sengupta, and S. Chakravorty. 2016. Monsoons to mixing in the Bay of Bengal: Multiscale air-sea interactions and monsoon predictability. *Oceanography* 29(2):18–27, http://dx.doi.org/10.5670/oceanog.2016.35.

Jensen, T.G., H.W. Wijesekera, E.S. Nyadjro, P.G. Thoppil, J.F. Shriver, K.K. Sandeep, and V. Pant. 2016. Modeling salinity exchanges between the equatorial Indian Ocean and the Bay of Bengal. *Oceanography* 29(2):92–101, http://dx.doi.org/10.5670/oceanog.2016.42.

Jinadasa, S.U.P., I. Lozovatsky, J. Planella-Morató, J.D. Nash, J.A. MacKinnon, A.J. Lucas, H.W. Wijesekera, and H.J.S. Fernando. 2016. Ocean turbulence and mixing around Sri Lanka and in adjacent waters of the northern Bay of Bengal. *Oceanography* 29(2):170–179, http://dx.doi.org/10.5670/oceanog.2016.49.

Johnston, T.M.S., D. Chaudhuri, M. Mathur, D.L. Rudnick, D. Sengupta, H.L. Simmons, A. Tandon, and R. Venkatesan. 2016. Decay mechanisms of near-inertial mixed layer oscillations in the Bay of Bengal. *Oceanography* 29(2):180–191, http://dx.doi.org/10.5670/oceanog.2016.50.

Joseph, P.V., K.P. Sooraj, C.A. Babu, and T.P. Sabin. 2005. A cold pool in the Bay of Bengal and its interaction with the active-break cycle of the monsoon. *CLIVAR Exchanges* 34(10):3.

Le Bouteiller, A., A. Leynaert, M.R. Landry, R. Le Borgne, J. Neveux, M. Rodier, J. Blanchot, and S.L. Brown. 2003. Primary production, new production, and growth rate in the equatorial Pacific: Changes from mesotrophic to oligotrophic regime. *Journal of Geophysical Research* 108, 8141, http://dx.doi.org/10.1029/2001JC000914.

Lee, C.M., S.U.P. Jinadasa, A. Anutaliya, L.R. Centurioni, H.J.S. Fernando, V. Hormann, M. Lankhorst, L. Rainville, U. Send, and H.W. Wijesekera. 2016. Collaborative observations of boundary currents, water mass variability, and monsoon response in the southern Bay of Bengal. *Oceanography* 29(2):102–111, http://dx.doi.org/10.5670/oceanog.2016.43.

MacKinnon, J.A., J.D. Nash, M.H. Alford, A.J. Lucas, J.B. Mickett, E.L. Shroyer, A.F. Waterhouse, A. Tandon, D. Sengupta, A. Mahadevan, and others. 2016. A tale of two spicy seas. *Oceanography* 29(2):50–61, http://dx.doi.org/10.5670/oceanog.2016.38.

Mahadevan, A., G. Spiro Jaeger, M. Freilich, M. Omand, E.L. Shroyer, and D. Sengupta. 2016. Freshwater in the Bay of Bengal: Its fate and role in air-sea heat exchange. *Oceanography* 29(2):72–81, http://dx.doi.org/10.5670/oceanog.2016.40.

Marra, J. 1992. Diurnal variability in chlorophyll fluorescence: Observations and modeling. Conference volume 1750, Ocean Optics XI, July 19, 1992, San Diego, CA, *Proceedings of SPIE - The International Society for Optical Engineering*, http://dx.doi.org/10.1117/12.140654.

Moum, J.N., and J.D. Nash. 2009. Mixing measurements on an equatorial ocean mooring. *Journal of Atmospheric and Oceanic Technology* 26(2):317–336, http://dx.doi.org/10.1175/2008JTECHO617.1.

Pant, V., M.S. Girishkumar, T.V.S. Udaya Bhaskar, M. Ravichandran, F. Papa, and V.P. Thangaprakash. 2015. Observed interannual variability of near-surface salinity in the Bay of Bengal. *Journal of Geophysical Research* 120(5):3,315–3,329, http://dx.doi.org/10.1002/2014JC010340.

Papa, F., F. Durand, W.B. Rossow, A. Rahman, and S.K. Bala. 2010. Satellite altimeter-derived monthly discharge of the Ganga-Brahmaputra River and its seasonal to interannual variations from 1993 to 2008. *Journal of Geophysical Research* 115, C12013, http://dx.doi.org/10.1029/2009JC006075.

Pinkel, R., M.A. Goldin, J.A. Smith, O.M. Sun, A.A. Aja, M.N. Bui, and T. Hughen. 2011. The Wirewalker: A vertically profiling instrument carrier powered by ocean waves. *Journal of Atmospheric and Oceanic Technology* 28(3):426–435, http://dx.doi.org/10.1175/2010JTECHO805.1.

Rainville, L., and R. Pinkel. 2001. Wirewalker: An autonomous wave-powered vertical profiler. *Journal of Atmospheric and Oceanic Technology* 18(6):1,048–1,051, http://dx.doi.org/10.1175/1520-0426(2001)018<1048:WAAWPV>2.0.CO;2.

Sarkar, S., H.T. Pham, S. Ramachandran, J.D. Nash, A. Tandon, J. Buckley, A.A. Lotliker, and M.M. Omand. 2016. The interplay between submesoscale instabilities and turbulence in the surface layer of the Bay of Bengal. *Oceanography* 29(2):146–157, http://dx.doi.org/10.5670/oceanog.2016.47.

Sarma, V.V.S.S., G.D. Rao, R. Viswanadham, C.K. Sherin, J. Salisbury, M.M. Omand, A. Mahadevan, V.S.N. Murty, E.L. Shroyer, M. Baumgartner, and K.M. Stafford. 2016. Effects of freshwater stratification on nutrients, dissolved oxygen, and phytoplankton in the Bay of Bengal. *Oceanography* 29(2):222–231, http://dx.doi.org/10.5670/oceanog.2016.54.

Sengupta, D., S.R. Parampil, G.S. Bhat, V.S.N. Murty, V. Ramesh Babu, T. Sudhakar, K. Premkumar, and Y. Pradhan. 2008. Warm pool thermodynamics from the Arabian Sea Monsoon Experiment (ARMEX). *Journal of Geophysical Research* 113, C10008, http://dx.doi.org/10.1029/2007JC004623.

Sengupta, D., and M. Ravichandran. 2001. Oscillations of Bay of Bengal sea surface temperature during the 1998 summer monsoon. *Geophysical Research Letters* 28(10):2,033–2,036, http://dx.doi.org/10.1029/2000GL012548.

Shankar, D., S.R. Shetye, and P.V. Joseph. 2007. Link between convection and meridional gradient of sea surface temperature in the Bay of Bengal. *Journal of Earth System Science* 116:385–406, http://dx.doi.org/10.1007/s12040-007-0038-y.

Shroyer, E.L., D.L. Rudnick, J.T. Farrar, B. Lim, S.K. Venayagamoorthy, L.C. St. Laurent, A. Garanaik, and J.N. Moum. 2016. Modification of upper-ocean temperature structure by subsurface mixing in the presence of strong salinity stratification. *Oceanography* 29(2):62–71, http://dx.doi.org/10.5670/oceanog.2016.39.

Smith, J.A., R. Pinkel, M. Goldin, O. Sun, S. Nguyen, T. Hughen, M. Bui, and A. Aja. 2012. Wirewalker dynamics. *Journal of Atmospheric and Oceanic Technology* 29(1):103–115, http://dx.doi.org/10.1175/JTECH-D-11-00049.1.

Vinayachandran, P.N., V.S.N. Murty, and V. Ramesh Babu. 2002. Observations of barrier layer formation in the Bay of Bengal during summer monsoon. *Journal of Geophysical Research* 107(C12), 8018, http://dx.doi.org/10.1029/2001JC000831.

Wang, X.J., M. Behrenfeld, R. Le Borgne, R. Murtugudde, and E. Boss. 2009. Regulation of phytoplankton carbon to chlorophyll ratio by light, nutrients and temperature in the Equatorial Pacific Ocean: A basin-scale model. *Biogeosciences* 6:391–404, http://dx.doi.org/10.5194/bg-6-391-2009.

Weller, R.A., J.T. Farrar, J. Buckley, S. Mathew, R. Venkatesan, J. Sree Lekha, D. Chaudhuri, N. Suresh Kumar, and B. Praveen Kumar. 2016. Air-sea interaction in the Bay of Bengal. *Oceanography* 29(2):28–37, http://dx.doi.org/10.5670/oceanog.2016.36.

ACKNOWLEDGMENTS

This work was accomplished with Office of Naval Research support under the umbrella of the Air-Sea Interactions Regional Initiative (ASIRI). AJL was specifically supported by ONR Grant N00014-13-1-0489. Many thanks to Captain Chris Curl, June Marion, Jonathan Ladner, and the crew of R/V *Roger Revelle* for the field support necessary to collect the observations presented here. The ONR-ASIRI project has benefited greatly from the collaborative efforts of investigators from India and Sri Lanka.

AUTHORS

Andrew J. Lucas (ajlucas@ucsd.edu) is Assistant Research Oceanographer, Scripps Institution of Oceanography, University of California, San Diego, La Jolla, CA, USA. **Jonathan D. Nash** is Professor, College of Earth, Ocean, and Atmospheric Sciences, Oregon State University, Corvallis, OR, USA. **Robert Pinkel** is Professor Emeritus, Scripps Institution of Oceanography, University of California, San Diego, La Jolla, CA, USA. **Jennifer A. MacKinnon** is Professor, Scripps Institution of Oceanography, University of California, San Diego, La Jolla, CA, USA. **Amit Tandon** is Professor of Mechanical Engineering, University of Massachusetts Dartmouth, North Dartmouth, MA, USA. **Amala Mahadevan** is Senior Scientist, Woods Hole Oceanographic Institution, Woods Hole, MA, USA. **Melissa M. Omand** is Assistant Professor, Graduate School of Oceanography, University of Rhode Island, Narragansett, RI, USA. **Mara Freilich** is a graduate student in the MIT/WHOI Joint Program in Oceanography, Cambridge/Woods Hole, MA, USA. **Debasis Sengupta** is Professor, Centre for Atmospheric and Oceanic Sciences, Indian Institute of Science, Bangalore, India. **M. Ravichandran** is Head, Observations and Modeling, Indian National Centre for Ocean Information Services, Hyderabad, India. **Arnaud Le Boyer** is Postdoctoral Scholar Oceanographer, Scripps Institution of Oceanography, University of California, San Diego, La Jolla, CA, USA.

ARTICLE CITATION

Lucas, A.J., J.D. Nash, R. Pinkel, J.A. MacKinnon, A. Tandon, A. Mahadevan, M.M. Omand, M. Freilich, D. Sengupta, M. Ravichandran, and A. Le Boyer. 2016. Adrift upon a salinity-stratified sea: A view of upper-ocean processes in the Bay of Bengal during the southwest monsoon. *Oceanography* 29(2):134–145, http://dx.doi.org/10.5670/oceanog.2016.46.